Hybrid Nanomembranes for High Power and High Energy Density Supercapacitors and Their Yarn Application

Jae Ah Lee,[†] Min Kyoon Shin,[†] Shi Hyeong Kim,[†] Seon Jeong Kim,[†,*] Geoffrey M. Spinks,[‡] Gordon G. Wallace,[‡] Raquel Ovalle-Robles,[§] Márcio D. Lima,[§] Mikhail E. Kozlov,[§] and Ray H. Baughman[§,*]

[†]Center for Bio-Artificial Muscle and Department of Biomedical Engineering, Hanyang University, Seoul 133-791, South Korea, [‡]ARC Centre of Excellence for Electromaterials Science, Intelligent Polymer Research Institute, University of Wollongong, Wollongong, NSW, 2522, Australia, and [§]The Alan G. MacDiarmid NanoTech Institute, University of Texas at Dallas, Richardson, Texas 75083, United States

ABSTRACT

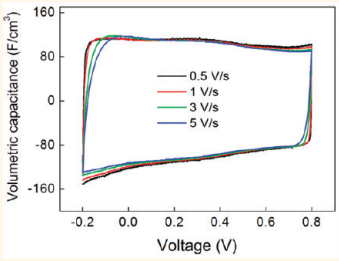

We report mechanically robust, electrically conductive, free-standing, and transparent hybrid nanomembranes made of densified carbon nanotube sheets that were coated with poly (3,4-ethylenedioxythiophene) using vapor phase polymerization and their performance as supercapacitors. The hybrid nanomembranes with thickness of ~66 nm and low areal density of ~15 μg/cm^2 exhibited high mechanical strength and modulus of 135 MPa and 12.6 GPa, respectively. They also had remarkable shape recovery ability in liquid and at the liquid/air interface unlike previous carbon nanotube sheets. The hybrid nanomembrane attached on a current collector had volumetric capacitance of ~40 F/cm^3 at 100 V s^{-1} (~40 and ~80 times larger than that of onion-like carbon measured at 100 V s^{-1} and activated carbon measured at 20 V s^{-1}, respectively), and it showed rectangular shapes of cyclic voltammograms up to ~5 V s^{-1}. High mechanical strength and flexibility of the hybrid nanomembrane enabled twisting it into microsupercapacitor yarns with diameters of ~30 μm. The yarn supercapacitor showed stable cycling performance without a metal current collector, and its capacitance decrease was only ~6% after 5000 cycles. Volumetric energy and power density of the hybrid nanomembrane was ~70 mWh cm^{-3} and ~7910 W cm^{-3}, and the yarn possessed the energy and power density of ~47 mWh cm^{-3} and ~538 W cm^{-3}.

KEYWORDS: carbon nanotube sheets · conducting polymer · supercapacitor electrodes · free-standing nanomembranes · yarn supercapacitor

Ultrathin (thickness <100 nm) electrically conducting membranes can be used as electrodes for sensors, actuators, optical devices, fuel cells, scaffolds for assembling nanoparticles, and separation of biological macromolecules.[1−6] Various approaches have been suggested for the fabrication of free-standing nanomembranes based on organic polymers and/or inorganic materials: spin-casting of films,[7] layer-by-layer assembly of polyelectrolyte multilayers,[8] cross-linking of self-assembled monolayers,[9] and assembly of triblock copolymers.[10,11] Loading materials such as gold nanoparticles[12] or carbon nanotubes[13] make membranes robust and electrically conductive. However, these methods are often time-consuming and have some limitations in terms of achievable electrical and electrochemical membrane performance as well as scale-up. Alternative approaches are needed for the preparation of mechanically robust, free-standing, conductive nanomembranes that could be easily manufactured.

Carbon nanotube aerogel sheets drawn from multiwalled carbon nanotube forests provide an excellent platform for the formation of conductive and transparent membranes. Carbon nanotube aerogel sheets densified by ethanol vapor turn into carbon nanotube sheets (CNSs) with well-aligned nanotube structures and thickness of ~50 nm.[14] These densified CNSs have unique properties in optical transparency, electrical conductance, mechanical strength, and density: the transmittance for densified sheets is over 85% for light polarized perpendicular to the alignment direction;[14] the sheet resistances in the aligned direction and in the transverse direction are ~600 Ω/sq and ~15 kΩ/sq, respectively;[15] a stack of densified sheets has specific tensile strength of 465 MPa/(g/cm^3);[14] and the density and areal density of densified sheets are typically ~1.5 mg/cm^3 and ~3 μg/cm^2, respectively.[14,16] However, despite the potential suggested by these remarkable properties, a major problem is that the membranes irreversibly collapse into isolated bundles upon withdrawal through liquid or liquid/air interfaces,[16,17] limiting

* Address correspondence to sjk@hanyang.ac.kr, rbaughmn@utdallas.edu.

Received for review September 22, 2011 and accepted December 14, 2011.

Published online December 14, 2011
10.1021/nn203640a

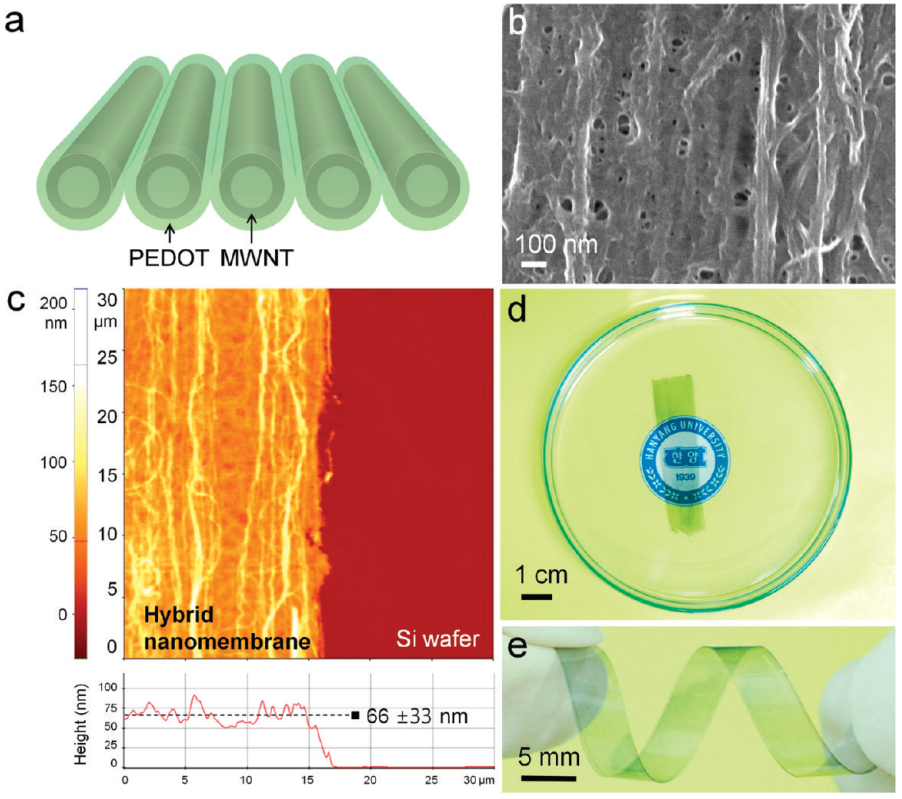

Figure 1. PEDOT/CNS hybrid nanomembranes prepared by VPP. (a) Schematic representation of a PEDOT-coated CNS nanomembrane. (b) SEM image showing the morphology of a hybrid nanomembrane. (c) AFM image showing the surface morphology and a height profile for a hybrid nanomembrane on a Si wafer, which provided an average nanomembrane thickness of 66 nm. The thickness variation for the hybrid nanomembrane was determined from the root-mean-square of heights. (d) Photo image of a free-standing and optically transparent hybrid nanomembrane in ethanol. (e) Photo image of a helically twisted hybrid nanomembrane/PET film. The hybrid nanomembrane was directly attached to a PET film by VPP without transfer. All hybrid nanomembranes were prepared from a densified one-layer CNS, and the loading of PEDOT in the membranes was 85 wt %.

their use in applications such as electrolyte-filled capacitors.

In this work, we have developed mechanically robust, electrically conductive, free-standing, and transparent hybrid nanomembranes made of densified CNSs that were coated with poly(3,4-ethylenedioxythiophene) (PEDOT) using vapor phase polymerization (VPP). The hybrid nanomembrane has remarkable shape recovery ability, and it can be transformed into flexible and strong yarns with microscale diameters employing a simple twisting method. We also show electrochemical performance of prepared nanomembranes and yarns needed for supercapacitor applications.

RESULTS AND DISCUSSION

VPP is a versatile technique capable of providing highly conducting polymer coatings on both conducting and nonconducting substrates.[18] The VPP method consists of coating the substrate with an oxidant dissolved in solution and exposure of the coated surface to appropriate monomer vapor.[19] This method is very useful in producing conductive thin membranes on substrates with highly controllable properties.[20] The high electrical conductivity, optical transparency, chemical stability, and electrocatalytic properties of PEDOT[21] have enabled its applications as electrochemical, ion-selective or mechanical sensors, transparent electrodes, and as fuel cell electrodes.[22−24] The fabrication process is summarized in Figure 1a. Stacked carbon nanotube aerogel sheets were used as the platform to support the PEDOT VPP product. The investigated CNSs contained a one- or two-layer stack of carbon nanotube aerogel sheets, which were densified by contact with dilute oxidant solution (8 wt % oxidant in butanol) and subsequent evaporation of the butanol. The PEDOT content in the hybrid nanomembranes was controlled by varying the oxidant concentration.

Scanning electron microscope (SEM) and atomic force microscope (AFM) images indicate that the oriented fibrous structure of the nanotube sheets is retained after VPP (Figure 1b,c). Hybrid nanomembranes containing 85 wt % PEDOT were obtained using a 8 wt % oxidant solution. The average thickness of a one-layer CNS/85 wt % PEDOT nanomembrane (~66 nm, as shown in Figure 1c) was slightly larger than that of a one-layer CNS densified by butanol

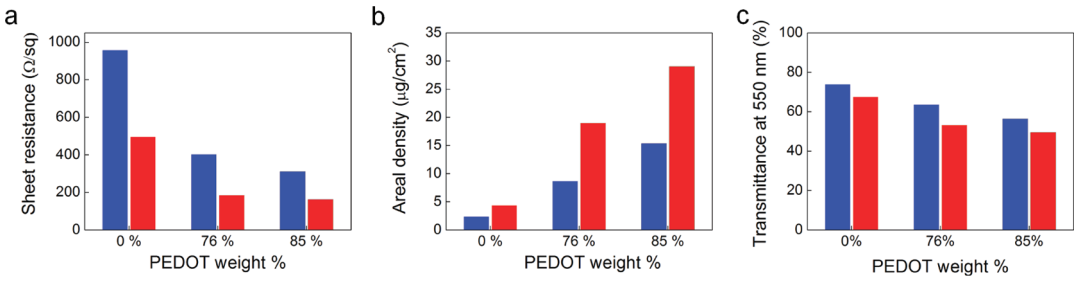

Figure 2. (a) Electrical sheet resistance, (b) areal density, and (c) optical transmittance at 550 nm for carbon nanotube membranes containing differing numbers of CNS layers and amounts of PEDOT. Blue rectangles are for one-layer CNS/PEDOT nanomembranes, and red rectangles are for two-layer CNS/PEDOT nanomembranes.

(~52 nm) and about one-half of that for a two-layer CNS/85 wt % PEDOT nanomembrane (~112 nm) (Supporting Information, Figure S1).

The sheet resistance of the hybrid nanomembranes decreased with increasing PEDOT content (Figure 2a). A hybrid nanomembrane consisting of 85 wt % PEDOT and a one-layer CNS had a sheet resistance of 312 Ω/sq, which was three times lower than that of the one-layer CNS densified by butanol (958 Ω/sq). This decrease in sheet resistance is attributed to the thin PEDOT layer providing an electronically conducting connection between individual CNTs, as shown in Figure 1b,c. The areal density of a two-layer CNS/85 wt % PEDOT nanomembrane (29 μg/cm^2) was almost twice that of a one-layer CNS/85 wt % PEDOT nanomembrane (15 μg/cm^2) (Figure 2b). Correspondingly, the sheet resistance of the two-layer-based hybrid nanomembrane (163 Ω/sq) was about one-half of that for the one-layer-based hybrid nanomembrane containing the same 85 wt % PEDOT (312 Ω/sq).

Hybrid nanomembranes (containing one or two CNS layers), which were peeled from the glass slide after VPP, were optically transparent and free-standing in ethanol (Figure 1d). The transmittance of the one-layer CNS/85 wt % PEDOT was 56% (at 550 nm wavelength) and 18% lower than for a one-layer CNS densified by butanol (74%) (Figure 2c). This decreased transparency is due to the filling of the voids between CNTs by the PEDOT and an increase in membrane thickness. However, the hybrid nanomembrane still has moderately high optical transparency (Figure 1d,e), although the transparency of the hybrid nanomembrane is lower than that of commercial ITO films (80−90% for 7−400 Ω/sq).[25,26] Moreover, the transparency of the hybrid nanomembrane is comparable to that of the transparent graphene film (thickness: ~50 nm) fabricated for supercapacitors (~50% for 8−10 S/cm).[27] The hybrid nanomembrane can be directly prepared on a flexible and transparent substrate such as poly(ethylene terephthalate) (PET) without the need for transfer after deposition of the as-drawn sheet. The flexibility of the hybrid membrane/PET film and its excellent adhesion to the PET substrate enabled a ribbon of the hybrid membrane/PET sheet stack to be twisted into helical shape without causing structural damage (Figure 1e).

To investigate the mechanical and structural robustness of hybrid nanomembranes, we carried out tensile tests, sheet resistance changes as a function of bending curvature, and structure deformation tests in a liquid and at a liquid/air interface. Figure 3a shows a stress−strain curve of a one-layer CNS/85 wt % PEDOT nanomembrane. The specific mechanical strength and modulus of the hybrid nanomembranes were 51 ± 3 MPa/(g/cm^3) and 5.1 ± 2.9 GPa/(g/cm^3), respectively. When we calculated mechanical properties using the average thickness of hybrid nanomembranes obtained from AFM, the mechanical strength and modulus were 135 ± 8 MPa and 12.6 ± 5.3 GPa, respectively. This mechanical strength was ~3 times higher than that of 30 μm thick poly(4-styrene sulfonate)-doped PEDOT films (43 MPa).[28] Moreover, the strength and modulus of the one-layer CNS/85 wt % PEDOT nanomembrane exceeded other nanomembrane structures fabricated by self-assembly (ultimate strengths of up to 100 MPa and moduli of 1−10 GPa).[29−32]

We also investigated electrical resistance changes as a function of bending curvature for a hybrid nanomembrane (one-layer CNS/85 wt % PEDOT) (Figure 3b). The electrical resistance changes were below 0.1% up to a bend curvature of 0.2 mm^{-1}. Generally, conducting polymers are very brittle, particularly for thin films.[33] The brittleness often generates a dramatic increase in resistance upon deformation. The present results show that PEDOT−CNT composites provide the insensitivity of electronic transport to bending that is needed for applications as flexible electrodes.

Unsupported CNSs irreversibly collapse into a fiber when withdrawn from a liquid. However, unlike CNSs, the hybrid nanomembranes show a remarkable shape-memory effect. While a hybrid nanomembrane collapsed into a yarn when drawn from an ethanol bath, the sheet shape was recovered when the hybrid nanomembrane was reimmersed into the ethanol bath. Though shape recovery is imperfect, reversible transition between sheet and yarn structures occurred during numerous cycles of withdrawal from the liquid bath and reimmersion in this bath (Figure 3c).

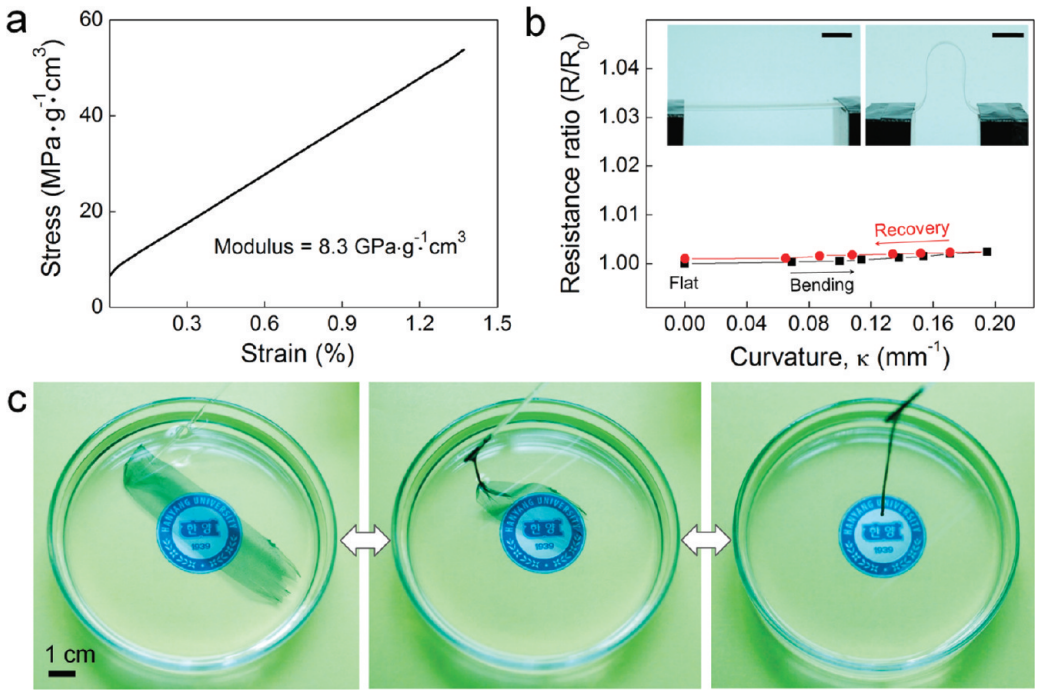

Figure 3. Mechanical and structural robustness of hybrid nanomembranes. (a) Stress−strain curve for a self-supported hybrid nanomembrane. (b) Dependence of normalized electrical resistance on curvature for a hybrid nanomembrane attached to a 100 μm thick PET film (the plotted resistances are average values obtained from three cycles of bending and unbending, and R_0 and R are the resistances of the planar and bent membranes, respectively). The insets are pictures of the flat and bent samples (scale bar: 1 cm). (c) Photo images showing shape reversibility of a hybrid nanomembrane: free-standing nanomembrane in ethanol (left), nanomembrane partially drawn from the ethanol (middle), and fully collapsed nanomembrane after complete removal from the ethanol (right). The arrows indicate that shape recovery of a collapsed nanomembrane is possible by reimmersing the membrane in ethanol. The PEDOT weight percent was 85%, and a one-layer CNS was used for hybrid nanomembrane preparation.

In addition, hybrid nanomembranes suspended by the edges of a wire paper clip passed through the ethanol/air interface without structural collapse into a fiber (Supporting Information, Figure S2). These observations indicate that our hybrid nanomembranes are mechanically robust despite their nanoscale thicknesses and low areal densities of ~15 μg/cm^2.

The electrochemical capacitance of the hybrid nanomembranes attached to current collectors such as a glassy carbon electrode was determined in 1 M sulfuric acid using a three-electrode cell in which the nanomembranes were the working electrode, Pt mesh was the counter electrode, and Ag/AgCl was the reference electrode. The one-layer CNS/85 wt % PEDOT nanomembrane showed rectangular cyclic voltammograms (CVs) even at high scan rates of up to ~5 V s^{-1} (Figure 4a). The CV shape with the straight rectangular sides at such a high scan rate represents a very small ESR of the nanomembrane/glassy carbon electrode and the fast diffusion of electrolyte ions into the hybrid nanomembrane.[34] The Nyquist plot in the frequency range of 100 kHz to 10 mHz features a vertical curve, indicating a nearly ideal capacitive behavior (Supporting Information, Figure S3). The volumetric capacitance of hybrid nanomembranes was obtained using $(I_a + |I_c|) \times \Delta t/(2V\Delta E)$, where I_a and I_c are the anodic and cathodic voltammetric current on the anodic and cathodic scans, Δt is scan time, V is the volume of the hybrid nanomembrane, and ΔE is the potential range of the CV. In going from 0.01 to 100 V s^{-1}, the volumetric capacitances of the hybrid nanomembrane were 123 and 40 F/cm^3 (67 and 21.5 F/g for gravimetric capacitances), respectively (Figure 4b). This means that the hybrid nanomembrane is able to cycle at an ultrahigh scan rate of 100 V s^{-1}. The volumetric capacitance measured at 0.01 V s^{-1} is almost two times higher than that of the graphene-based supercapacitor (~60 F/cm^3).[35] A dependence of the discharge current on the scan rate was plotted in Figure 4c. A red line shows a linear dependence of the discharge currents, indicating low resistive contributions up to ~10 V s^{-1}. Evolution of the real and imaginary parts (C' and C'') of the electrochemical capacitance obtained from electrochemical impedance spectroscopy (Figure 4d) was plotted according to following equations:[36]

$$C'(\omega) = \frac{-Z''(\omega)}{\omega \times |Z(\omega)|^2}$$

$$C''(\omega) = \frac{-Z'(\omega)}{\omega \times |Z(\omega)|^2}$$

where ω is the angular frequency and Z' and Z'' are the real part and the imaginary part of the impedance,

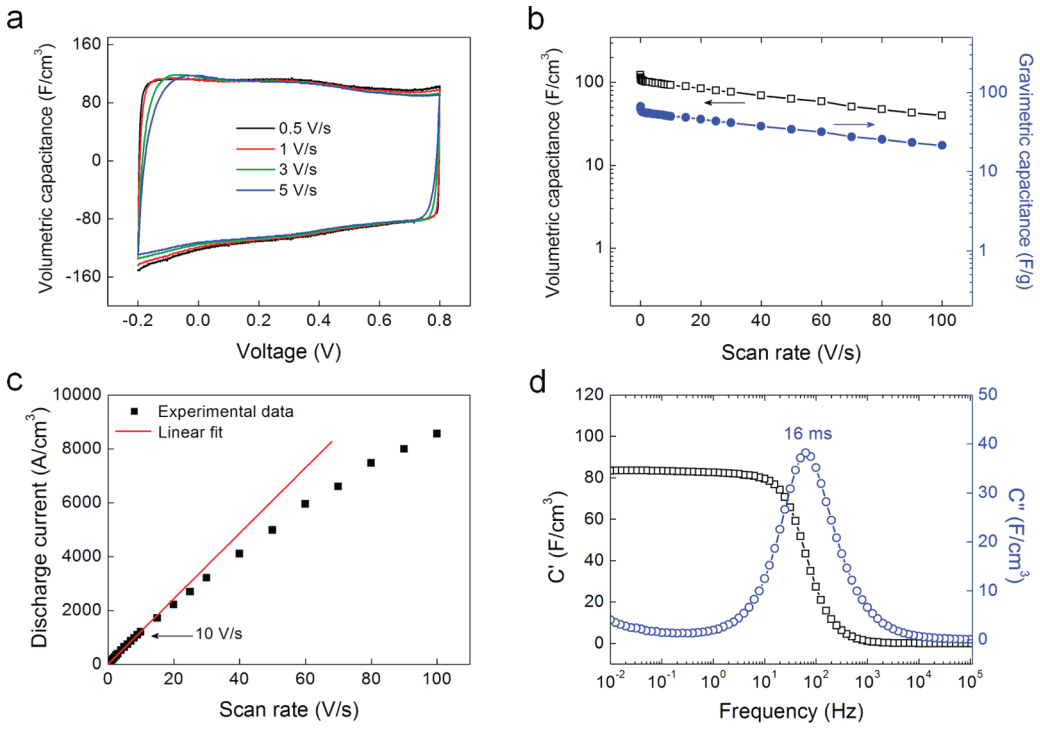

Figure 4. Electrochemical characterizations of hybrid nanomembranes. (a) CV curves at various scan rates ranging from 0.5 to 5 V s^{-1}. Rectangular shapes indicate the ideal capacitive behavior. (b) Volumetric and gravimetric capacitance *versus* scan rate. (c) Dependence of discharge currents on scan rates. A red line shows linear dependence up to 10 V s^{-1}. (d) Frequency response of the real (C') and imaginary (C'') volumetric capacitances of the hybrid nanomembrane. The relaxation time constant is 16 ms.

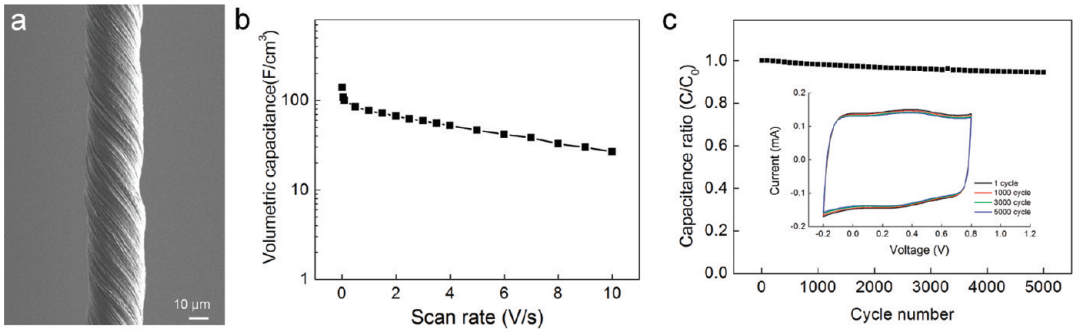

Figure 5. Yarn supercapacitor application of hybrid nanomembranes. (a) SEM image of a twisted yarn from a two-layer CNS/PEDOT nanomembrane. (b) Volumetric capacitance *versus* scan rate of the twisted yarn. (c) Cyclic stability of the twisted yarn at a scan rate of 500 mV s^{-1} in 1.0 M sulfuric acid. The inset shows no degradation of CVs during 5000 cycles.

defined as $Z'(\omega)^2 + Z''(\omega)^2 = |Z(\omega)|^2$. The electrochemical capacitance retention ability was also examined through relaxation time constants. The definition of the relaxation time constant is minimum time needed to discharge all of the energy from the sample with an efficiency of greater than 50%.[37] The time constant of hybrid nanomembrane was 16 ms, and the value is similar to that of the ultrahigh power microsupercapacitors with ~7 μm thick onion-like carbon layers (time constant = 26 ms)[38] and much lower than that of the onion-like carbon-based macroscopic supercapacitors (time constant >1000 ms).[37] From experimental results of Figure 4, we confirmed that the hybrid nanomembrane can be well adhered on a current collector by simple attachment without a polymer binder and has the potential for delivering high power and energy.

High strength and flexibility of our nanomembranes enable twisting them into microyarns with diameters of ~30 μm, as shown in Figure 5a. Although fibers for miniaturized microsupercapacitors have been fabricated using rolling-up technology based on the release of nanoscale thick membranes from substrates,[39] direct yarn fabrication from nanomembranes without a MEMS technique is for the first time reported. Figure 5b shows capacitance performance of a yarn twisted from a two-layer CNS/85 wt % PEDOT membrane at scan rates ranging from 0.01 to 10 V s^{-1}. CVs of the twisted yarn were measured without a metal current collector.

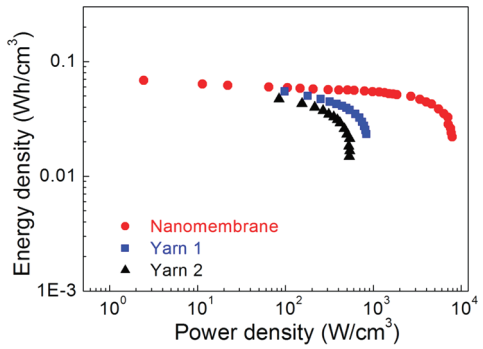

Figure 6. Ragone plots of the hybrid nanomembrane and yarns. Yarn 1 and yarn 2 are the carbon black imbedded yarn and simple twisted yarn, respectively. The capacitance of the yarns was measured without metal current collectors.

Although capacitance decrease was observed, the yarn is still applicable as high power and energy density capacitors. The twisted yarn exhibited high cyclic stability, as shown in Figure 5c. The electrochemical capacitance decrease was only ~6% up to 5000 cycles, maintaining rectangular shapes of CV curves (the inset of Figure 5c).

Energy and power densities of hybrid nanomembrans and their twisted yarns are highlighted in Figure 6. The electrochemical performance described in the Ragone plot was based on the volume of the nanomembrane and yarn and calculated from CV curves according to the following equations.[38] For a given scan rate ν (V s^{-1}), the discharged power P (W) was calculated by integrating the current (I) *versus* potential (E) plots:

$$P = \int_{-0.2}^{0.8} I \times E dE$$

The discharged energy W (Wh) was obtained by using the following equation:

$$W = \frac{\Delta E}{\nu \times 3600} \int_{-0.2}^{0.8} I \times E dE$$

where ΔE is the discharge potential range (1 V). The hybrid nanomembrane exhibited power density of ~7910 W cm^{-3} (~4391 kW kg^{-1}) and energy density of ~70 mWh cm^{-3} (~37 Wh kg^{-1}). The gravimetric energy density of the hybrid nanomembrane was almost twice that of the transparent graphene nanofilm (thickness = ~50 nm) supercapacitor,[27] and the power density was at least 130 times higher. The twisted yarn from the nanomembrane showed volumetric power and energy density of ~538 W cm^{-3} and ~47 mWh cm^{-3} (the value was measured without a metal current collector). The hybrid nanomembranes can be twisted containing guest materials such as carbon black. After incorporation of carbon black into twisted yarns, electrochemical performance was enhanced. The power and energy densities of carbon black imbedded yarns was ~836 W cm^{-3} and ~55 mWh cm^{-3}. Excellent electrochemical properties of our samples come from nanoscale thickness of membranes which provides high surface area and effective ion accessibility during electrochemistry.

CONCLUSIONS

We have developed robust and free-standing conductive nanomembranes based on CNSs and a conducting polymer. The mechanical robustness enabled reversible transition between membrane and yarn structures, reflecting a remarkable shape-memory effect of hybrid nanomembranes. For a thickness of ~66 nm, the hybrid nanomembranes exhibited sheet resistances below 200 ohm per square, moderate optical transparency of 56% at 550 nm wavelength, high flexibility and minor changes in resistance upon bending. When the hybrid nanomembrane was attached to a conducting substrate, the nanomembrane was operable at an ultrahigh scan rate of 100 V s^{-1}. The twisted yarn from the hybrid nanomembrane also showed high cyclic stability and high capacitive performance at fast charge/discharge rates. The nanomembrane and twisted yarn had excellent power and energy density (~7910 W cm^{-3} and ~70 mWh cm^{-3} for the nanomembrane, ~538 W cm^{-3} and ~47 mWh cm^{-3} for the yarn). On the basis of these results, the hybrid nanomembranes and twisted yarns seem applicable to sensors, actuators, optical devices, and fuel cells, as well as electrochemical capacitors.

MATERIALS AND METHODS

Materials. The aligned arrays of carbon multiwalled nanotubes (MWNT forests) were grown on a Si wafer using chemical vapor deposition.[40] Iron(III) *p*-toluenesulfonate hexahydrate (Fe(III)PTS, M_w = 677.52), pyridine (anhydrous, 99.8%), 1-butanol (for molecular biology, ≥99%), and 3,4-ethylenedioxythiophene (EDOT) monomer (97%) were purchased from Sigma-Aldrich (USA), and 2 N sulfuric acid solutions (1 M H_2SO_4) were purchased from Daejung Chemicals (South Korea).

Fabrication of Hybrid Nanomembranes. A 20 wt % Fe(III)PTS/butanol solution was used as an oxidizing agent. Pyridine (1.6 vol %) was added to the 20 wt % Fe(III)PTS/butanol solution. The Fe(III)PTS/pyridine/butanol solution containing from 1 to 8 wt % of the oxidant was made by diluting the stock solution containing 20 wt % oxidant in butanol. The diluted solutions (70 μL for 75 mm × 7 mm CNSs) were dropped over one- or two-layer carbon nanotube aerogel sheets. The carbon nanotube aerogel sheets were allowed to dry at 60 °C for 20 min to evaporate the butanol. Densified CNSs with a thickness of ~50 nm were subsequently obtained. The EDOT monomer was cast on both sides of the densified CNSs in a VPP chamber, and then the samples were exposed to EDOT vapor at 60 °C for 1 h. After polymerization, the samples were removed from the VPP chamber. Finally, the nanomembrane was thoroughly rinsed three times in ethanol to remove unreacted oxidant.

Fabrication of Twisted Yarns. The hybrid nanomembranes were twisted into strong and flexible yarns using electric motor devices. For preparing twisted yarns containing carbon black, carbon black dispersed in deionized water was deposited on

the hybrid nanomembrane by a simple dropping method, and then the membrane was twisted.

Characterization. Surface morphology and height profiles of hybrid nanomembranes were obtained using scanning electron microscopy (Hitachi S4700, Japan) and atomic force microscopy (Park Systems XE-100, South Korea). Galvanostatic, potentiostatic, and electrochemical impedance measurements were measured using a Gamry instrument (reference 600, USA). Two-probe sheet resistance measurements were performed using a digital multimeter (Fluke Corporation, Model 187, USA), and two-probe bending resistance changes were measured using a homemade bending-recovery device.

Acknowledgment. Supported by the Creative Research Initiative Center for Bio-Artificial Muscle of Education, Science and Technology (MEST) and MEST-US Air Force Cooperation Program (Grant No. 2011-00178) in Korea and the Air Force Grant AOARD-10-4067 and Robert A. Welch Foundation Grant AT-0029 in the United States.

Supporting Information Available: Details of AFM analysis, photo images of hybrid membranes attached to a clip wire, and a Nyquist plot. This material is available free of charge *via* the Internet at http://pubs.acs.org.

REFERENCES AND NOTES

1. Jiang, C.; Markutsya, S.; Pikus, Y.; Tsukruk, V. V. Freely Suspended Nanocomposite Membranes as Highly Sensitive Sensors. *Nat. Mater.* **2004**, *3*, 721–728.
2. Birkholz, M.; Ehwald, K.-E.; Kulse, P.; Drews, J.; Fröhlich, M.; Haak, U.; Kaynak, M.; Matthus, E.; Schulz, K.; Wolansky, D. Ultrathin TiN Membranes as a Technology Platform for CMOS-Integrated MEMS and BioMEMS Devices. *Adv. Funct. Mater.* **2011**, *21*, 1652–1656.
3. Strassner, M.; Esnault, J. C.; Leroy, L.; Leclereq, J. -L.; Garrigues, M.; Sagnes, I. Fabrication of Ultrathin and Highly Flexible InP-Based Membranes for Microoptoelectromechanical Systems at 1.55 μm. *Photonics Technol. Lett.* **2005**, *17*, 804–806.
4. Zhu, X.; Zhang, H.; Zhang, Y.; Liang, Y.; Wang, X.; Yi, B. An Ultrathin Self-Humidifying Membrane for PEM Fuel Cell Application: Fabrication, Characterization, and Experimental Analysis. *J. Phys. Chem. B* **2006**, *110*, 14240–14248.
5. Mueggenburg, K. E.; Lin, X.-M.; Goldsmith, R. H.; Jaeger, H. M. Elastic Membranes of Close-Packed Nanoparticle Arrays. *Nat. Mater.* **2007**, *6*, 656–660.
6. Striemer, C. C.; Gaborski, T. R.; McGrath, J. L.; Fauchet, P. M. Charge- and Size-Based Separation of Macromolecules Using Ultrathin Silicon Membranes. *Nature* **2007**, *445*, 749–753.
7. Elbaccouch, M. M.; Shukla, S.; Mohajeri, N.; Seal, S.; T-Raissi, A. Microstructural Analysis of Doped-Strontioum Cerate Thin Film Membranes Fabrication *via* Polymer Precursor Technique. *Solid-State Ionics* **2007**, *178*, 19–28.
8. Ko, Y. H.; Kim, Y. H.; Park, J.; Nam, K. T.; Park, J. H.; Yoo, P. J. Electric-Field-Assisted Layer-by-Layer Assembly of Weakly Charged Polyelectrolyte Multilayers. *Macromolecules* **2011**, *44*, 2966–2872.
9. Cheng, W.; Campolongo, M. J.; Tan, S. J.; Luo, D. Free-standing Ultrathin Nano-membranes *via* Self-Assembly. *Nano Today* **2009**, *4*, 482–493.
10. Zhao, D.; Yang, P.; Chmelka, B. F.; Stucky, G. D. Multiphase Assembly of Mesoporous-Macroporous Membranes. *Chem. Mater.* **1999**, *11*, 1174–1178.
11. Gonzales-Perez, A.; Castelletto, V.; Hamley, I. W.; Taboada, P. Biomimetic Triblock Copolymer Membranes: From Aqueous Solutions to Solid Supports. *Soft Matter* **2011**, *7*, 1129–1138.
12. Singamaneni, S.; Jiang, C.; Merrick, E.; Kommireddy, D.; Tsukruk, V. V. Robust Fluorescent Response of Micropatterned Multilayered Films. *J. Macromol. Sci., Part B* **2007**, *46*, 7–19.
13. Kang, T. J.; Cha, M.; Jang, E. Y.; Shin, J.; Im, H. U.; Kim, Y.; Lee, J.; Kim, Y. H. Ultra-thin and Conductive Nanomembrane Arrays for Nanomechanical Transducers. *Adv. Mater.* **2008**, *20*, 3131–3137.
14. Zhang, M.; Fang, S.; Zakhidov, A. A.; Lee, S. B.; Aliev, A. E.; Williams, C. D.; Atkinson, K. R.; Baughman, R. H. Strong, Transparent, Multifunctional, Carbon Nanotube Sheets. *Science* **2005**, *309*, 1215–1219.
15. Kuznetzov, A. A.; Lee, S. B.; Zhang, M.; Baughman, R. H.; Zakhidov, A. A. Electron Field Emission from Transparent Multiwalled Carbon Nanotube Sheets for Inverted Field Emission Displays. *Carbon* **2010**, *48*, 41–46.
16. Aliev, A. E.; Lima, M. D.; Fang, S.; Baughman, R. H. Underwater Sound Generation Using Carbon Nanotube Projectors. *Nano Lett.* **2010**, *10*, 2374–2380.
17. Zhang, X.; Jiang, K.; Feng, C.; Liu, P.; Zhang, L.; Kong, J.; Zhang, T.; Li, Q.; Fan, S. Spinning and Processing Continuous Yarns from 4-Inch Wafer Scale Super-Aligned Carbon Nanotube Arrays. *Adv. Mater.* **2006**, *18*, 1505–1510.
18. Winther-Jensen, B.; Chen, J.; West, K.; Wallace, G. Vapor-Phase Polymerization of 3,4-Ethylenedioxythiophene: A Route to Highly Conducting Polymer Surface Layers. *Macromolecules* **2004**, *37*, 4538–4543.
19. Truong, T. L.; Kim, D.-O.; Lee, Y.; Lee, T.-W.; Park, J. J.; Pu, L.; Nam, J.-D. Surface Smoothness and Conductivity Control of Vapor-Phase Polymerized Poly(3,4-ethylenedioxythiophene) Thin Coating for Flexible Optoelectronic Applications. *Thin Solid Films* **2008**, *516*, 6020–6027.
20. Kim, J.; Kim, E.; Won, Y.; Lee, H.; Suh, K. The Preparation and Characteristics of Conductive Poly(3,4-ethylenedioxythiophene) Thin Film by Vapor-Phase Polymerization. *Synth. Met.* **2003**, *139*, 485–489.
21. Wang, Y. Research Progress on a Novel Conductive Polymer—Poly(3,4- ethylenedioxythiophene) (PEDOT). *J. Phys.* **2009**, *152*, 012023.
22. Yoon, H.; Jang, J. Conducting-Polymer Nanomaterials for High-Performance Sensor Applications: Issues and Challenges. *Adv. Funct. Mater.* **2009**, *19*, 1567–1576.
23. Xia, Y.; Ouyang, J.; PEDOT, P. S. S. Films with Significantly Enhanced Conductivities Induced by Preferential Solvation with Cosolvents and Their Application in Polymer Photovoltaic Cells. *J. Mater. Chem* **2011**, *21*, 4927–4936.
24. Winther-Jensen, B.; Winther-Jensen, O.; Forsyth, M.; Macfarlane, D. R. High Rates of Oxygen Reduction over a Vapor Phase-Polymerized PEDOT Electrode. *Science* **2008**, *321*, 671–674.
25. www.cpfilms.com.
26. www.delta-technologies.com.
27. Yu, A.; Roes, I.; Davies, A.; Chen, Z. Ultrathin, Transparent, and Flexible Graphene Films for Supercapacitor Application. *Appl. Phys. Lett.* **2010**, *96*, 253105.
28. Lang, U.; Naujoks, N.; Dual, J. Mechanical Characterization of PEDOT:PSS Thin Films. *Synth. Met.* **2009**, *159*, 473–479.
29. Jiang, C.; Rybak, B. M.; Marcutsya, S.; Kladitis, P. E.; Tsukruk, V. V. Self-Recovery of Stressed Nanomembranes. *Appl. Phys. Lett.* **2005**, *86*, 121912.
30. Markutsya, S.; Jiang, C.; Pikus, Y.; Tsukruk, V. V. Freely Suspended Layer-by-Layer Nanomembranes: Testing Micromechanical Properties. *Adv. Funct. Mater.* **2005**, *15*, 771–780.
31. Fery, A.; Dubreuil, F.; Möhwald, H. Mechanics of Artificial Microcapsules. *New J. Phys.* **2004**, *6*, 18.
32. Vinogradova, O. I. Mechanical Properties of Polyelectrolyte Multilayer Microcapsules. *J. Phys.: Condens. Matter* **2004**, *16*, R1105–R1134.
33. Wang, L.; Lin, T.; Wang, X.; Kaynak, A. Frictional and Tensile Properties of Conducting Polymer Coated Wool and Alpaca Fibers. *Fibers Polym.* **2005**, *6*, 259–262.
34. Conway, B. E. *Electrochemical Supercapacitors; Scientific Fundamentals and Technological Applications*; Kluwer Academic/Plenum Publishers: New York, 1999.
35. Zhu., Y.; Murali, S.; Stoller, M. D.; Ganesh, K. J.; Cai, W.; Ferreira, P. J.; Pirkle, A.; Wallace, R. M.; Cychosz, K. A.; Thommes, M.; Su, D.; Stach, E. A.; Ruoff, R. S. Carbon-Based Supercapacitors Produced by Activation of Graphene. *Science* **2011**, *332*, 1537–1541.

36. Taberna, P.-L.; Simon, P.; Fauvarque, J. F. Electrochemical Characteristics and Impedance Spectroscopy Studies of Carbon−Carbon Supercapacitors. *J. Electrochem. Soc.* **2003**, *150*, 292–300.
37. Portet, C.; Yushin, G.; Gogotsi, Y. Electrochemical Performance of Carbon Onions, Nanodiamonds, Carbon Black and Multiwalled Nanotubes in Electrical Double Layer Capacitors. *Carbon* **2007**, *45*, 2511–2518.
38. Pech, D.; Brunet, M.; Durou, H.; Huang, P.; Mochalin, V.; Gogotsi, Y.; Taberna, P.-L.; Simon, P. Ultrahigh-Power Micrometre-Sized Supercapacitors Based on Onion-like Carbon. *Nat. Nanotechnol.* **2010**, *5*, 651–654.
39. Schmidt, O. G.; Everl, K. Nanotechnology: Thin Solid Films Roll Up into Nanotubes. *Nature* **2001**, *410*, 168.
40. Zhang, M.; Atkinson, K. R.; Baughman, R. H. Multifunctional Carbon Nanotube Yarns by Downsizing an Ancient Technology. *Science* **2004**, *306*, 1358–1361.